Influences of Lake Malawi

on the spatial and diurnal variability of local precipitation

Shunya Koseki[1] and **Priscilla A. Mooney**[2]

1: Geophysical Institute, University of Bergen, Bjerknes Centre for Climate Research, Bergen, Norway

2: NORCE Norwegian Research Centre, Bjerknes Centre for Climate Research, Bergen, Norway

Corresponding author: Shunya Koseki

Email: Shunya.Koseki@gfi.uib.no

Address: Allégate 70, 5007, Bergen, Norway

Abstract

We investigate how the intensity and spatial distribution of precipitation varies around Lake Malawi on a diurnal time scale, which can be valuable information for water resource management in tropical southeastern African nations. Using a state-of-the-art satellite product and regional atmospheric model, the well-defined diurnal cycle is detected around Lake Malawi with harmonic and principle component analyses: the precipitation is intense during midnight to morning over Lake Malawi and the precipitation peaks in the daytime over the surrounding area. This diurnal cycle in the precipitation around the lake is associated with the lake-land breeze circulation. Comparisons between the benchmark simulation and an idealized simulation in which Lake Malawi is removed, reveals that the diurnal variations in precipitation are substantially amplified by the presence of Lake Malawi. This is most evident over the lake and surrounding coastal regions. Lake Malawi also enhances the lake-land breeze circulation; the nocturnal lakeward land breeze generates surface convergence effectively and precipitation intensifies over the lake. Conversely, the daytime landward lake breeze generates the intense divergence over the lake and precipitation is strongly depressed over the lake. The lake-land breeze and the background vapour enriched by Lake Malawi drives primarily a diurnal variation in the surface moisture flux divergence/convergence over the lake and surrounding area which contributes to the diurnal cycle of precipitation in this region.

1. Introduction

A key climatological characteristic of tropical southeastern Africa is the manifestation of dry and wet seasons induced by the meridional march of the Inter-tropical Convergence Zone (ITCZ). This seasonal movement in the ITCZ is associated with the southwesterly Indian summer and northeasterly winter monsoons (e.g., Camberlin 1997; Viste and Sorteberg, 2013; Jury 2016; Diallo et al., 2018; Koseki and Bhatt, 2018) as shown in Figs. S1a-l. In summer (May to September), tropical southeasten Africa is covered entirely with a moisture flux divergence (Fig. S1m) and consequently, a dry season falls on this region. The northeastward moisture flux provides some of the summer precipitation over northeastern Africa and South Asia (e.g., Segele et al., 2009a; Viste and Sorteberg, 2013; Gleixner et al., 2017; Bohlinger et al., 2017). Conversely, the southwestward Indian winter monsoon generates a large convergence of vertically-integrated moisture flux over the tropical southeast of Africa (November to March, as shown Fig. S1n) bringing a wet season to this region. This monsoon-brought precipitation is very important for the regional economy and society of the southeastern African nations such as Tanzania, Mozambique, Madagascar, and Malawi where their economies depend highly on rain-fed agriculture.

Variability in hourly rainfall is also dominant over Southeastern Africa. It is controlled largely by a diurnal cycle due to the thermal heat contrast between water surface and land surface in the tropics (e.g., Estoque, 1967; Mak and Walsh, 1976; Kikuchi and Wang, 2008; Teo et al., 2011; Koseki et al., 2013; Jury, 2016). The diurnal cycle is observed ubiquitously around the tropical coastal areas since the thermal contrast between coastal land and ocean during daytime and nighttime,

induces the sea and land breeze circulation (e.g., Kitoh and Arakawa, 2005; Kikuchi and Wang, 2008; Teo et al., 2011; Diro et al., 2012; Koseki et al., 2013). Steep terrain and land-lake contrast also generate the similar diurnal variations in precipitation. These variations are associated with the diurnal cycle of mountain-valley and lake-land breeze systems (e.g., Keen and Lyons, 1978; Joseph et al., 2008; Stivari et al, 2003; Crosman and Horel, 2010; Koseki et al., 2018). Such information on diurnal variation in precipitation is highly important for efficient water resource management in nations with economies that depend strongly on rain.

Lake Malawi, located at 12.11°S and 34.22°E (Fig. S1), is the third largest of the African Great Lakes and ninth in the world having an area of 29,600 km^2, a maximum width of 75km, and a maximum length of 560km. Lake Malawi is an important water resource for surrounding tropical southeastern African nations such as Malawi, Mozambique and Tanzania (Kumambala and Ervine, 2010). In particular, a large part of agriculture and energy in Malawi originates from the water resource of Lake Malawi and the Shire River which flows from the lake; all of the national hydropower stations are built on the Shire River (a total installation capacity of 280MW; Kumambala and Ervine, 2010) and the largest national sugar plantations are supplied with water from the Shire River. Societies along the Shire River and surrounding Lake Malawi are exposed to high risks of flooding during the rainy season (November to March, Fig. 1) when the lake level is high due to rainfall over the lake (e.g., Neuland, 1984; Schäfer et al., 2015). Regarding other aspects, Lake Malawi is an important fishing resource in Malawi and it has a very unique ecosystem and biodiversity (e.g., Weyl et al., 2010). Lake Malawi itself plays an important role in the regional climate system. Diallo et al. (2018) performed climate simulations with a state-of-the-art regional climate model and suggested that Lake Malawi is a

75 water source for regional precipitation (over the lake and surrounding area) via
76 intense latent heat flux release from the lake surface.

77 Although Diallo et al. (2018) have investigated the role of Lake Malawi for
78 monthly time scales, little is known about the diurnal cycle of rainfall around Lake
79 Malawi and the lakes's influence on the diurnal cycle. In general, the African Great
80 Lakes play an important role for the regional hydrological weather and climate system
81 as a large water source. For example, Thiery et al. (2016) showed that Lake Victoria
82 (area of 59,947km^2), which is the largest African Great Lake, triggers extreme
83 thunderstorm over the lake during nighttime. Other exampes include severe
84 snowstorms around the Great Lakes of North America (area of 244,106km^2) (e.g.,
85 Sousonis and Mann, 2000; NOrato et al., 2013), and local precipitation induced by
86 Lake Chad (area of 25,000km^2) (Lauwaet et al., 2012). Since Lake Malawi, a large
87 water body (29,600km^2), is located in the tropics, the region can be affected by the
88 strong diurnal cycle of incoming solar radiation (e.g., Crosman and Horel, 2010). This
89 is the main driver of the diurnal variations in precipitation and local breeze systems.
90 Although it is expected that Lake Malawi can drive local circulation in response to the
91 diurnal solar radiation, the lake's role in the diurnal cycle of precipitation is less clear
92 and poorly understood. This is partly due to the lack of tools to study this topic but
93 recent developments in the resolution of numerical models now permit such
94 investigations.

95 This study aims to investigate the regional diurnal cycle of precipitation in the
96 rainy season (November to March) and quantify the effects of Lake Malawi on the
97 diurnal cycle of precipitation using state-of-the-art observational products and
98 numerical regional model. Using a satellite product with a relatively coarse spatial
99 resolution, a climatological diurnal cycle is overviewed and a case study of November

100 to March in 2014/15 is investigated using a higher resolution satellite product for the
101 purpose of evaluating the numerical simulation.

102 The rest of this paper is structured as follow: Section 2 gives the details of
103 observational data and numerical model used in this study and statistical
104 methodologies to investigate the diurnal variations. Section 3 provides the results of
105 the statistical analysis on the observations and numerical simulation including an
106 assessment of the modeled diurnal cycle. Moreover, the results of an idealized
107 numerical experiment will be used to elucidate the physical mechanisms that underlie
108 Lake Malawi's role in the diurnal cycle of precipitation around the lake. Section 4
109 will discuss the details of the simulation results focusing on the quantification of the
110 influence of Lake Malawi and finally, we will summarize this study in Section 5.
111

112 **2. Data, Model, and Methodology**

113 *2.1 Observational Data*

114 Satellite observations are obtained from both the Tropical Rainfall Measuring
115 Mission (Huffman et al., 2007) version 3B42 (TRMM 3B42) and the Global
116 Precipitation Measurement (GPM, Skofronick-Jackson et al., 2017) mission data
117 (Level-3). TRMM 3B42 has a high temporal coverage (1998-2014) which facilitates a
118 climatological overview of the diurnal cycle over Lake Malawi. However, the spatial
119 resolution of TRMM 3B42 (0.25°) prohibits its use in the analysis of the spatial
120 characteristics of the diurnal cycle over the lake and its shores. This difficulty is
121 overcome by using GPM, the successor to TRMM 3B42, which has a higher spatial
122 resolution of 0.1°. This facilitates a more detailed study of spatial variations in the
123 diurnal cycle of precipitation. The temporal resolution of the original GPM Level-3
124 data is every 30 minutes which is averaged to hourly rainfall in this study.

125

126 *2.2 Weather Research and Forecasting (WRF) Model*

127 The Advanced Research Weather Research and Forecasting (hereafter referred
128 to WRF, Skamarock et al., 2007) model version 3.9.1 is used to investigate the diurnal
129 variations around Lake Malawi. The domains used in all simulations are shown in
130 Figure 1a. The outer domain covers southeastern Africa, -20.74902°S to -2.958107°S
131 and 23.3115°E to 44.0885°E with 15km grid spacings (171×117 grids) and the inner
132 domain is centred on Lake Malawi, -15.87943°S to -8.219772°S and 32.22042°E to
133 37.06839°E with 3km grid spacing (155×250 grids), respectively (Fig. 2a). Both
134 domains have 56 vertical layers. The outer domain is forced laterally with 6 hourly
135 ERA-Interim (Dee et al., 2011) data which has a grid spacing of 0.75° and at the
136 lower boundary by the daily Optimum Interpolated Sea Surface Temperature (OISST,
137 Reynolds et al., 2007) which has a grid spacing of 0.25°. The inner domain is forced
138 laterally by the outer domain of WRF (the outer domain of WRF does not interact
139 with the inner domain).

140 The following physical schemes are used in our WRF simulations: the WRF
141 Single-moment (WSM) 6-class scheme for microphysics (Hong and Lim, 2006) and
142 the Yonsei University parameterization for the Planetary Boundary Layer (PBL;
143 Hong et al., 2006). The longwave and shortwave radiative forcing are parameterized
144 by the Rapid Radiative Transfer Model (Mlawer et al., 1997) schemes. Betts-Miller-
145 Janjíc (Janjíc, 1994) scheme is used for parameterizing convective processes in the
146 outer domain only; cumulus parameterization is switched off in the convection
147 permitting inner domain. A study of the sensitivity of precipitation in this region to
148 the convective schemes used in the outer domain showed that simulations using the
149 Betts-Miller-Janjíc scheme reproduced the observed precipitation over land better

than simulations using the Kain-Fritsch (Kain, 2004) scheme (not shown). Therefore, the Betts-Miller-Janjíc scheme is chosen for the outer domain in this study with no cumulus scheme used in the inner, high-resolution domain. Over the land and lake grids that are based on MODIS landuse data, the NOAH land surface model consisting of 4-layers (Chen and Dudhia, 2001a, b) and the 9-layer lake model (Xu et al., 2016) are implemented and air-land/lake interactions are active in the simulations.

With the model configurations above, a control experiment is initialized on the 1st January 2014 at 00 UTC of ERA-Interim for atmosphere and land surface and integrated until April 1st of 2015 (referred to WRF-CTL, hereafter). This run will compliment the observations to gain insights into the diurnal variations around Lake Malawi. In a second experiment, the grid boxes over Lake Malawi are converted from water to land grid boxes (Figs. 1b and c). This facilitates an exploration of the role of Lake Malawi on the local diurnal variations (called WRF-NOLM in the rest of the paper). Due to this conversion, some land surface properties are modified in WRF-NOLM: the landuse index of the converted grids is set to be savanna which is the most dominant landuse category in the inner domain of WRF experiments. The soil type of the converted grids is also replaced with sandy clay loam which is the majority soil type for the savanna grids in the inner domain. Additionally, the surface albedo over Lake Malawi grids is set to a value of albedo averaged over the savanna grids in the inner domain. Finally, the soil moisture and temperature of the converted grids are initialized by averaged value of savanna grids. These modifications are done only in the inner domain to avoid any modulations in larger-scale meteorological and hydrological quantities associated with the absence of Lake Malawi. All settings of the outer domain of WRF-NOLM are exactly the same as those of WRF-CTL.

We analyze the hourly output of the 5 months from November in 2014 to March in 2015; that is the first 10 months are designated as a spin-up period for initialising the land surface following the methodologies of Cosgrove et al. (2002) and Chen et al. (2007). In particular, in WRF-NOLM, the soil moisture and temperature are initialized with an averaged value, which is to a large extent artificial. Therefore, a long spin-up period is employed for initialising the land surface.

2.3 Methodologies to detect the nature of diurnal variation

Harmonic analysis has been widely used to quantify the main characteristics of the diurnal cycle (e.g., Yang and Slingo, 2001; Diro et al., 2012; Mooney et al., 2017). One particular advantage of harmonic analysis is the estimation of the explained variance (%) of a specific frequency and its phase from a time series. This study follows Mooney et al. (2017) by fitting the following function to the NDJFM-averaged hourly data,

$$R(t) \cong a_{24}\cos\left(\frac{2\pi(t-\phi_{24})}{24}\right) + a_{12}\cos\left(\frac{2\pi(t-\phi_{12})}{12}\right) \quad (1),$$

where $R(t)$ is the hourly variation of total rainfall and a_{24} (a_{12}) and ϕ_{24} (ϕ_{12}) are the amplitude and phase of the diurnal and semi-diurnal cycle, respectively.

The empirical orthogonal function (EOF) analysis is additionally used to capture the features of the diurnal cycle around Lake Malawi following previous studies (e.g., Kikuchi and Wang, 2008; Teo et al., 2011).

The EOF analysis is used to identify the dominant spatio-temporal patterns. For the diurnal cycle, it is known that the first mode represents a stationary dipole pattern between coastal land and ocean while the second mode identifies a propagation pattern from land to sea (the EOF patterns and principle component

198 scores between the first and second modes are out of phase by approximately $\pi/4$,
199 e.g., Kikuchi and Wang, 2008; Teo et al., 2011). Employing these statistical
200 methodologies, we will explore the details of the observed and modeled diurnal cycle
201 around Lake Malawi in Section 3.2 and 3.3. The EOF analysis is adopted into the
202 diurnal deviation components with,

203 $$A'(t) = A(t) - \overline{A} \qquad (2),$$

204 where A is a variable and t is time (hourly). The overbar and prime denote the daily-
205 mean and daily-deviated components, respectively.

206

207 **3. Results**

208 In this section, we will show the essential features of diurnal cycle of
209 precipitation around Lake Malawi using satellite observations and WRF simulations.
210 Additionally, the results of the idealized WRF simulation will be compared and
211 contrasted with the control simulation to reveal the role of Lake Malawi in the local
212 diurnal cycle of precipitation.

213

214 *3.1 Climatology*

215 Firstly, we take an overview of the climatological diurnal cycle of
216 precipitation around Lake Malawi using TRMM 3B42 which has good temporal
217 coverage but relatively coarse resolution (temporarily and spatially). Figure 2
218 illustrates the 3-hourly precipitation obtained by TRMM-3B42 for NDJFM-mean
219 climatology. Between 00-03 to 06-09 UTC (02-05 to 08-11 LST), the precipitation
220 over Lake Malawi is enhanced and the precipitation over the surrounding land area
221 becomes weaker. At 09-12 UTC, the precipitation is suppressed over the entire area.
222 Later, from 12-15 LST, precipitation is activated over the land surrounding Lake

223 Malawi. The land precipitation intensifies widely at 15-18 UTC while rainfall over
224 Lake Malawi is negligible. From 18-21 to 21-00 UTC, the land precipitation is
225 gradually reduced and precipitation over Lake Malawi commences. That is, around
226 Lake Malawi there is a well-organized diurnal variation in precipitation. Interestingly,
227 the magnitude of land and lake precipitation is almost identical (0.9 mm/h).
228
229 *3.2 Case study, 2014/15 NDJFM*
230 In this subsection, the more detailed nature of the diurnal cycle, which is
231 indicated in the preceding subsection, is investigated with a finer resolution satellite
232 product and numerical simulation for a case study of November to March in 2014/15.
233 Figures 3a-e show monthly-mean rainfall for GPM from November to March. In
234 November, the daily rainfall around Lake Malawi is low compared to the other
235 months. There is little rainfall over the Southern part of Lake Malawi but there is
236 some intense rainfall over the northern part of the lake. Rainfall becomes more
237 intense in December particularly over the centre of Lake Malawi. Precipitation peaks
238 in January and it is very intense in the entire domain with rainfall over Lake Malawi
239 reaching ~ 22 mm/h. From February to March, the precipitation over land decreases
240 while the lake precipitation over the lake remains strong, especially, in the central
241 area (around 18 mm/h). The precipitation over Lake Malawi is not distributed
242 homogeneously, but it seems that there is a dependency on location: the precipitation
243 is intense in the central part of the lake in December to March, in particular, the
244 precipitation spreads broadly around the centre of the lake. In the northern and
245 southern edges of the lake, there are also moderate peaks of the precipitation in
246 Feruary and March. These distributions might be determined by several factors (for
247 example, lake surface temperature), which is a highly complex process and beyond

248 the scope of this study. Fig. 3f-j show that WRF-CTL can capture the seasonal march
249 of larger-scale precipitation. However, the land precipitation tends to be
250 overestimated, in particular, from January to February. This overestimation might be
251 due to the high topography (higher than 2300m) around Lake Malawi (see section 4).
252 WRF-CTL successfully reproducse the intense lake precipitation from November to
253 March.
254
255 *3.3 Harmonic analysis*
256 Figure 4 shows the key characteristics of the diurnal cycle of precipitation
257 obtained by harmonics analysis (see Section 2.3) for NDJFM-mean hourly data of
258 GPM and WRF-CTL. Over Lake Malawi, the GPM observed sub-daily variations are
259 dominated by the diurnal cycle as shown in Fig. 4a (about 70-80% of explained
260 variance). Other dominant diurnal cycles are seen along the coast of Lake Malawi and
261 to the northeast of Lake Malawi, around 10°S and 35-36°E with a similar explained
262 variance. In WRF-CTL the dominant diurnal variation are captured well over Lake
263 Malawi with 60-70 % of explained variance in Fig. 4e. Although the strength of the
264 diurnal signal over the coastal region tends to be underestimated to some extent, the
265 terrestrial diurnal cycle is well represented in WRF-CTL in terms of the explained
266 variance.
267 The largest amplitudes of the diurnal cycle (a_{24} in Eq. 1) are observed over
268 Lake Malawi (up to 0.5 mm/h) and its coastal region (Fig. 4b). Over land, the
269 amplitude is relatively large to the northeast of the Lake (0.2-0.3 mm) where the
270 diurnal cycle dominates the sub-daily variations (Fig. 4a). This distribution of
271 amplitude is fairly well simulated by WRF-CTL in Fig. 4f. However, over Lake
272 Malawi, the amplitude is lower than observed while the amplitude over land to the

Northeast is too large (0.5 mm). This is consistent with the overestimated monthly-mean precipitation in Fig. 3. The observed phase of the diurnal cycle (ϕ_{24} in Eq. 1) shows a clear contrast over the lake and land in Fig. 4c; the maximum peak of the precipitation is at 02-03 UTC over the lake and surrounding coastal area and at 13-14 UTC over the land north of the lake where terrestrial precipitation is relatively large (Figs. 4a and b). This result is consistent with the climatological overview in the previous subsection. The timing of the WRF-simulated diurnal cycle in Fig. 4g agrees reasonably with that of the observations. Over the lake, the peak time is slightly late especially in the south (at 03-05 UTC) compared to the observations and the land precipitation is maximized at 13-14 UTC to the north of the lake. However, over the central eastern coastal region, the timing of the rainfall is incorrectly simulated.

In Figs. 4d and h, the explained variance of semi-diurnal cycle is given for GPM and WRF-CTL. Neither product shows a clear semi-diurnal cycle around Lake Malawi although there are some spots with relatively high variance of 40-50 %. These results suggest that the sub-daily variations in rainfall are mainly associated with the diurnal cycle over and around the lake while semi-diurnal cycle is almost negligible.

Figures 4i-l show the characteristics of the diurnal cycle of precipitation calculated by the harmonic analysis (Eq.1) for WRF-NOLM. Compared to WRF-CTL (Fig. 4e), the explained variance of the diurnal cycle is almost identical around Lake Malawi, in particular, to the northeast of the lake. Over the lake, the variance of the diurnal cycle is reduced remarkably in the southern part of the lake, which drops down to 20-30% in Fig. 5i (50-60% in WRF-CTL, shown in Fig. 4e). To the north of the lake, the diurnal cycle persists despite the absence of the lake. However, the amplitude of the diurnal cycle shrinks over the entire lake in Fig. 4j. Most notably, the reduction is largest in the central part and the northern part of the lake (a decrease

298 from 0.5 mm/h to 0.1-0.2 mm/h) even though the variance of the diurnal cycle is still
299 comparable to the WRF-CTL case. Over land, the diurnal amplitude is largely
300 unchanged when Lake Malawi is removed; this is most evident overland to the
301 northeast of the lake. The phase of the diurnal cycle is also modified over the lake. Its
302 peak is slightly earlier (around 02-03 UTC) than WRF-CTL (comparison between
303 Fig. 4g and 4k). In the southern shore of the lake (where the diurnal cycle almost
304 disappears), the phase is noisy with respect to WRF-CTL. The component of the
305 semi-diurnal cycle is almost identical with that in WRF-CTL and the semi-diurnal
306 cycle is not of importance in the sub-daily variations (Fig. 4l).
307
308 *3.4 EOF analysis*
309 The dominant spatio-temporal pattern of variation is provided through the
310 EOF analysis in Fig. 5. The EOF first mode of GPM shows a clear contrast between
311 the land and lake (Fig. 5a). The amplitude is larger over the lake than over the land
312 suggesting that the lake rainfall is more intense than the land rainfall. The coastal land
313 rainfall synchronizes with the lake rainfall in both eastern and western shores. This
314 mode explains 53.69 % of the total variance and its principal component (PC) score
315 (Fig. 5h) shows a distinct diurnal cycle. The peak of rainfall over land is between 12-
316 17 UTC and that of the lake rainfall over the lake is between 23-03 UTC. This seesaw
317 pattern of daytime rainfall over land and nighttime rainfall over the lake is quite
318 similar to the pattern described by sea-land contrast in the tropics (e.g., Teo et al.,
319 2011; Bhatt et al., 2016). The EOF second mode has 15.77% of the total variance and
320 its spatial pattern and PC score do not indicate a propagation mode from land to lake
321 (not shown). The PC score seems a semi-diurnal cycle and the spatial pattern is quite

322 spotty and it appears to be unrelated to Lake Malawi. Its amplitude is considerably
323 smaller than that of the first mode.

324 WRF-CTL represents well the sharp contrasting spatial pattern between the
325 land and lake in Fig. 5b as an EOF first mode (the explained variance is 41.51%).
326 However, as shown in Figs. 3 and 4, the amplitude of the land precipitation is
327 overestimated and coastal terrestrial rainfall synchronizing with the lake rainfall does
328 not spread widely compared to the observation although there is some coastal land
329 precipitation occurring simultaneously with the lake precipitation. While the PC score
330 of first mode is roughly consistent with that of observation (Figs. 5h and i), the phase
331 is somewhat shifted: the peak of the nighttime rainfall is around 03-07 UTC (later
332 than the observation) and that of daytime is around 12-14 UTC, which is slightly
333 earlier than the observation. In particular, the earlier simulated peak in the daytime
334 precipitation is a common issue in regional climate modeling (e.g., Nikulin et al.
335 2012; Pohl et al., 2014; Mooney et al., 2016, 2017; Koseki et al., 2018). Similar to the
336 GPM observations, WRF-CTL does not show any clear propagation mode by the
337 second mode and the large variation is limited in some small areas (its variance is
338 18.36 %) although the PC score of the second mode is lagged by approximately $\pi/4$
339 (not shown).

340 The modeled surface zonal wind shows an interesting distribution by the EOF
341 first mode in Fig. 5c: the lake shore is encompassed by the narrow bands of the
342 negative and positive daily anomalies of surface zonal wind (77.88% of the total
343 variance) and those bands spread over Lake Malawi. Combined with its PC score it
344 can be interpreted that the outgoing flow from the Lake is maximized between 09-13
345 UTC (Fig. 5i) and the incoming flow into the Lake is dominant between 21-03 UTC.
346 This diurnal-varying circulation is consistent with a well-characterized lake-land

breeze (e.g., Keen and Lyons, 1978; Crosman and Horel, 2010). The PC score of the surface zonal wind leads that of the precipitation by approximately 3 hours. The surface meridional wind also shows a remarkable pattern by the EOF first mode (61.46% of the total variance) in Fig. 5d: with a macroscopic view, there is a dipole mode of positive in the north and negative in the south of Lake Malawi. Combining it with the PC score (Fig. 5i), there is an outgoing/incoming flow of meridional surface wind during daytime/nighttime respectively. The EOF 1st mode of meridional wind varies approximately with the zonal wind as shown in Fig. 5i.

The EOF 1st mode also shows substantial changes in the diurnal cycle in WRF-NOLM as shown in Figs. 5e-g; the dipole pattern between the lake and surrounding terrestrial area almost disappears in the EOF 1st mode and the dominant variability is only over the land in Fig. 5e. The variance is still 35.60% and the amplitude over the land is almost identical with that of WRF-CTL in Fig. 5b. While the harmonic analysis estimates the diurnal cycle independently at each grid cell, the EOF analysis calculates the most explainable variability in all the selected grids and therefore, the amplitude at one grid would be affected by that at other grids. That is, in Fig. 5e, the variability at the lake grids are much smaller than those at land grids, which is consistent with the reduced amplitude of diurnal variation over the lake in Fig. 4j. The PC score indicates that the EOF 1st mode is a diurnal cycle in Fig. 5j with some modification in its peak time. Whereas the EOF 1st mode of surface zonal winds have the two narrow bands along the lake shore in WRF-NOLM (74.53% of the total variance), their spreads over the lake are largely diminished on both sides of the lake shore with respect to that in WRF-CTL (Figs. 5c and 5f). The magnitudes of the WRF-CTL (Fig. 5i) PC scores are similar to those for WRF-NOLM (Fig. 5j) and the maximum and minimum of the PC scores for both WRF-CTL and WRF-NOLM

372 occur during the day and the night, respectively. Similarly, the variability in surface
373 meridional wind is also reduced over the lake as shown in Fig. 5g. However, there is
374 still some evidence of a dipole pattern between the northern and southern part of Lake
375 Malawi as shown in WRF-CTL (Fig. 5d). However, the maximum of PC scores for
376 the meridional wind occurs slightly earlier in the WRF-NOLM (Fig. 5j) simulation
377 compared to the WRF-CTL (Figs. 5i).
378
379 *3.5 Nighttime and daytime precipitation*
380 As witnessed by the harmonic and EOF analyses above (Figs. 4-5), Lake
381 Malawi plays a crucial role in the generation and/or amplification of the diurnal cycle
382 of precipitation. At certain times in the day, the lake's role can be clearer than other
383 times (Fig. 6). During 00-03 UTC, the nocturnal precipitation occurs over Lake
384 Malawi in WRF-CTL (Fig. 6a) but this the lake-anchored precipitation is extensively
385 reduced in WRF-NOLM (Fig. 6b). Its influence is remarkable over the entire lake, in
386 particular, over the northern and central parts of the lake (Fig. 6c). This indicates the
387 importance of Lake Malawi for rainfall over the lake (as concluded by Diallo et al.,
388 2018). Conversely, the surrounding area of the lake experiences a modest reduction in
389 precipitation in the presence of the lake during midnight to early morning. During
390 daytime when the precipitation peak is closely tied to the maximum in local solar
391 heating (11-14 UTC), precipitation is more dominant over the surrounding area of the
392 lake than over the lake in WRF-CTL (Fig. 6d). While precipitation over the lake is
393 quite small, there is some increase in the precipitation over the southern part of the
394 lake in WRF-NOLM, (Fig. 6e). In contrast to the nocturnal precipitation, daytime
395 precipitation is amplified over the southern part of the lake although its response is
396 relatively weaker than that in the nighttime (Figs. 6c and f).

Figure 7 presents the surface horizontal wind and its divergence anomalies from daily-mean at nighttime and daytime, estimated by Eq. (2). In WRF-CTL, the incoming flow from the shore toward the lake is detected and the strong convergence forms over the lake shown in Fig. 7a. These lakeward flows are land breeze circulations and penetrate deeply into the lake as shown by the EOF analysis (Figs. 5c and d). The intense nocturnal rainfall (as in Fig. 6a) can be attributed to this strong convergence over the lake. In WRF-NOLM, the land breezes are extensively weakened and, as a result, the convergence over the lake shrinks considerably (Fig. 7b). The difference shows clearly that the intensification in the land breeze and convergence is due to Lake Malawi (Fig. 7c). While the daily-residual component of the surface wind can be seen not only around the lake but also in the region (Figs. 7a and b), the influence of the lake on the wind seems to be limited around and over the lake. During daytime, on the other hand, the outgoing flows, thus, lake breezes are organized well from the lake outward and this flow is highly divergent over the lake in WRF-CTL (Fig. 7d). This outgoing circulation can also be seen in WRF-NOLM (Fig. 7e), but its magnitude is considerably reduced and the flow-forming divergence is also reduced. The difference during daytime is almost a mirror image of that during nighttime and it shows that Lake Malawi plays an important role in the diurnal variations of local wind circulations. The lake surface seems to create a heat contrast favouring the lake-land breeze circulation in night- and daytime: the surface temperature over the lake is higher in WRF-CTL (25.7^{o}C) than in WRF-NOLM (24.8^{o}C) during nighttime and lower in WRF-CTL (26.8^{o}C) during the daytime than in WRF-NOLM (32.8^{o}C) This behaviour in the surface temperature can create favourable conditions for more convergence (divergence) and consequently, the precipitation over the lake is enhanced (suppressed) effectively.

3.6 Moisture flux convergence

The preceding subsections have shown that Lake Malawi radically drives the diurnal cycle in precipitation, and local circulations. Since the moisture flux, $\mathbf{U}q$, (here, $\mathbf{U}$ is horizontal wind vector and q is specific humidity at surface) due to the lake-land breeze circulations can be highly related to precipitation, we quantify the surface moisture flux and its diurnal variation. Note that 10m and 2m data are used for horizontal wind and specific humidity in this study. The moisture flux can be subdivided into four components like,

$$\mathbf{U}q(t) = \left(\overline{\mathbf{U}} + \mathbf{U}'(t)\right)\cdot\left(\overline{q} + q'(t)\right) = \overline{\mathbf{U}}\,\overline{q} + \overline{\mathbf{U}}q'(t) + \mathbf{U}'(t)\overline{q} + \mathbf{U}'(t)q'(t),$$

where the overbar and prime denote daily-mean and daily-deviation as Eq. 2. $\mathbf{U}$ is surface wind vector and q is surface specific humidity. The horizontal divergence of moisture flux is calculated as

$$\nabla\cdot\mathbf{U}q(t) = \underbrace{\nabla\cdot\overline{\mathbf{U}}\,\overline{q}}_{A} + \underbrace{\nabla\cdot\overline{\mathbf{U}}q'(t)}_{B} + \underbrace{\nabla\cdot\mathbf{U}'(t)\overline{q}}_{C} + \underbrace{\nabla\cdot\mathbf{U}'(t)q'(t)}_{D} \quad (3).$$

The term A is the moisture flux divergence/convergence due to daily-mean wind and humidity, which does not have diurnal variation, but its relevance is more to the moisture flux associated with the Indian winter monsoon over this region. The term B reflects the influence associated with the diurnal variation in the heat flux and the background wind. The term C indicates the contribution due to the lake-land breeze and the daily-mean humidity to the moisture flux divergence/convergence. The final term is attributed to the diurnal variations in local breeze and humidity. Since the term A does not contain any temporal change, only the three terms of B, C, and D are averaged over Lake Malawi and surrounding area as shown in Fig. 8a.

During nighttime, the moisture flux converges over Lake Malawi and diverges over the surrounding area mainly by the lake-land breeze circulation and background humidity in WRF-CTL (term C in Figs. 8b and c). The daily-mean (background) latent heat flux averaged over the lake grids is 155.2572 and 56.9174 W/m^2 for WRF-CTL and WRF-NOLM, respectively and the lake surface is an important water source of the local precipitation, depending on the wind conditions and other characteristics (e.g., topography). The intense moisture flux convergence is responsible for the nocturnal precipitation as shown in Fig. 8c. Other terms in Eq.3 do not substantially contribute to the moisture flux divergence/convergence. In WRF-NOLM, the diurnal varying breeze and background humidity also contributes to the moisture flux convergence/divergence, but its magnitude is much smaller than that in WRF-CTL in Figs. 8b and c. Consequently, the precipitation over the lake area is reduced without Lake Malawi. As shown in Fig. 6c, the precipitation surrounding the lake is somewhat enhanced in WRF-NOLM during nighttime (although the response of the rainfall is noisy and weak, the consistency with the response of the moisture flux is reasonable). During daytime, the lake-land breeze and background humidity are still the main driver of the moisture flux divergence/convergence over the lake and surrounding area in Figs. 8d and e. Without the lake, the divergence over the lake and convergence over the lake shore are weakened, which is consistent with the enhanced (reduced) daytime rainfall surrounding (over) the lake in WRF_CTL in Fig. 6f. The term *C* is mainly contributed by the zonal component, $\partial(uq)/\partial x$, which is about 70 to 80 % of the total divergence/convergence (not shown).

In both cases of nighttime and daytime, the other terms of *B* and *D* in Eq.3 do not contribute to the diurnal changes in moisture flux divergence/convergence. That is, the land-lake breeze and the enriched background water vapor due to Lake Malawi

mainly drive the diurnal variations in surface moisture flux and consequently, the precipitation around Lake Malawi.

4. Discussion

The previous section has revealed that Lake Malawi plays a vital role to form the diurnal variations in land-lake breeze systems and correspondingly, the precipitation. However, the diurnal cycle of surface winds do not completely disappear in WRF-NOLM, and there is still a signature of the diurnal cycle detected even in the absence of the lake. We provide a brief discussion on the possible other factors of the diurnal cycle around Lake Malawi.

While Lake Malawi is an active driver of the diurnal variations in the local land-lake breeze circulations, the local breeze circulation residually remains without Lake Malawi as shown in Fig. 7. As previous research (e.g., Tyson 1968a, 1968b and Koseki et al. 2018) has shown, complex terrain also induces a diurnal cycle in the mountain-valley breeze circulation whose mechanism is similar to that for sea-land and lake-land breezes. As shown in Fig. 9a, Lake Malawi is encompassed by the high-elevated terrain that is up to 2600m in the northeast. The altitude is below 600 m over all of Lake Malawi. This difference in the elevation forms the large gradients in the surface as shown in Figs. 9b and c. In particular, the two narrow bands of steep zonal gradient run along the eastern and western shore sides. These gradients can drive the down-hill mountain (incoming toward the lake) and uphill valley (outgoing from the lake shore) breeze circulations during nighttime and daytime respectively as shown in Fig. 5b, 7c and 7f. In addition to the lake shore, there are some steep gradients to the northeast (9°S and 34.5°E) and the southwest (14.5°S and 33.5-34.5°E). Around these high mountains, there are well-organized mountain and valley breeze circulation

during nighttime and daytime as in Figs. 7a, b, d and e. The daytime precipitation is enhanced around these regions, that is, the valley breeze can activate the cumulus convection and precipitation due to the topography-lifting effect (e.g., Joseph et al., 2008). The overestimated precipitation in the WRF simulations might be caused by an over sensitive response in convection to this valley breeze circulation.

As previously mentioned, the high topography around Lake Malawi can be another driver of the diurnal cycle around Lake Malawi. However, there could be some difference in timing between the diurnal cycle induced by the lake and mountain due to the difference in heat capacity. Therefore, in WRF_NOLM where the mountain is only a driver, the peak time of precipitation over the lake differs from that in WRF_CTL. That is, the diurnal cycle around Lake Malawi is a complicated system influenced by both the lake and the mountain. Similar mechanisms can be expected in other places where large lakes are surrounded by high mountains (e.g., Lake Tanganyika in Tanzania). Future work will investigate explicitly the role of high terrain in diurnal cycle of precipitation.

In our sensitivity experiment, we used only one land cover type and one soil type in the lake grid cells. This can slightly infleuce our results, as previous research (e.g., Bonan, 2008) has shown that changing the land cover from forests to open spaces (e.g., savanna or croplands) impacts precipitation and temperature. These differences are driven by changes in parameters associated with each land cover type, such as, albedo, surface roughness, leaf area index, and root depth. In tropical regions, changes from forest cover to grass decreases precipitation and increases temperature by changing the partitioning of the net surface radiation between latent and sensible heat fluxes (Bonan, 2008; Pitman et al., 2011). In particular, Semazzi and Song (2001) showed that changing the land cover type from forest to savanna grasslands

520 reduced precipitation over Mozambique. Consequently, changing the lake cover to a
521 tropical forest instead of svanna in our WRF-NOLM simulation would increase the
522 daytime precipitation in WRF-NOLM, potentially, altering the amplitude of the
523 diurnal cycle. However, it is unlikely that changing the land cover type to forest
524 would impact the phase of the diurnal cycle. Based on this, we hypothesise that
525 changing the lake to a forest cover type instead of savanna in WRF-NOLM, would
526 likely result in slightly smaller differences between WRF-CTL and WRF-NOLM with
527 respect to the amplitude of the diurnal cycle of precipitation but it would have no
528 impact on the phase of the diurnal cycle of precipitation. However, further studies on
529 the importance of the land cover change to the diurnal cycle of precipitation would be
530 necessary to test this hypothesis.

531 Cumulus convection and associated precipitation are also highly sensitive to
532 and modulated by soil moisture whose features are dependent on land use and soil
533 type (e.g., Walker and Rowntree, 1977; Pielke, 2001; Cook et al., 2006). For example,
534 Sugimoto and Takahashi (2017) suggested that the wetter soil moisture tends to
535 inhibit cumulus convection due to a lower sensible heat flux in South Asia during
536 Indian Summer Monsoon period. In our focusing area, the Indian Winter Monsoon
537 prevails and therefore, it can be anticipated that our results of precipitation and
538 cumulus convection will be changed when the different landuse and soil type are
539 employed in the lake grid cells. Additionally, we have tested only the homogenous
540 distribution of landuse and soil type in the lake grid boxes for the sensitivity
541 experiment. The heterogeneous distribution will modify the distribution of
542 precipitation over the lake. Therefore, further sensitivity experiments with difference
543 land use and soil type would be also interesting to investigate the characteristics of the
544 precipitation and land-atmosphere interactions in this region.

5. Concluding Remarks

In this study, we have investigated the diurnal variation of precipitation in summer (November to March) around Lake Malawi using the state-of-the-art satellite products and regional climate model. In a climatological view, TRMM-3B42 shows a clear diurnal cycle of precipitation around Lake Malawi: the precipitation over the lake is more enhanced during midnight to early morning while the surrounding land area experiences a daytime peak with identical amplitudes between the two phases. Such clear contrast between daytime rainfall over the land and nighttime rainfall over the lake can be found over Lake Victoria (Thiery et al., 2016), which is the largest great lake in the African Continent.

The spatially and temporally finer resolution satellite data of GPM and a convection permitting WRF simulation gives a more microscopic view of the diurnal varying precipitation in the area. A harmonic analysis reveals that the diurnal cycle of precipitation is largely dominant over Lake Malawi and to the northeast of the lake and their peak times are almost completely out of phase as suggested by TRMM-3B42. The WRF simulation can capture the diurnal variation in precipitation and reproduce realistic amplitudes of the lake rainfall whilst the land rainfall is overestimated. Analysis of the semi-diurnal cycle shows that the semi-diurnal component is a negligibly small contributor to the diurnal variations. The dominant diurnal variation can also be detected by the EOF analysis as a first principal component (the variance is almost half of the total variance). However, the second modes are not propagating pattern like those identified in Kikuchi and Wang (2008) and Teo et al. (2011). The surface winds also have the dominant first mode of EOF as

569 diurnal cycle. In particular, the lake-land breeze system is well generated along the
570 lake shore.

571 Without Lake Malawi, those diurnal variations in precipitation and lake-land
572 breeze are diminished substantially around Lake Malawi: a large part of the diurnal
573 variation in precipitation disappears over the lake region. The magnitude of the lake-
574 land breeze reduces its magnitude over the lake. During nighttime, the land breeze
575 does not penetrate deeply into the lake surface and convergence is not formed
576 effectively. During daytime, the outgoing lake breeze also shrinks and the divergence
577 over the lake is weakened considerably. As a result, the daytime rainfall over the
578 surrounding area becomes relatively moderate in the absence of the lake. Basically,
579 Lake Malawi creates a thermal contrast between the lake and land surface and this
580 contrast can drive a local lake-land breeze circulation (e.g., Steyn 2003; Kruit et al.,
581 2004; Crosman and Horel, 2010). As Diallo et al. (2018) suggested, Lake Malawi is a
582 source of water vapour and enhances the precipitation. The combination of lake-land
583 breeze and enriched background water vapour is the main contributor to the diurnal
584 cycle the surface moisture flux and consequently that in the precipitation.

585 Besides Lake Malawi, the steep gradient associated with high topographies
586 encompassing Lake Malawi also induces a diurnal cycle in the local circulation of the
587 mountain-valley breezes. Due to this breeze system, the diurnal cycle of the terrestrial
588 rainfall survives with identical amplitude in the presence and absence of Lake Malawi.
589 That is, the diurnal variation around Lake Malawi forms a combination of the two
590 independent systems of lake-land and mountain-valley breezes.

591 Based on the analysis of satellite observations and numerical simulations, we
592 conclude that Lake Malawi plays a central role in the remarkable diurnal cycle of
593 precipitation and local circulation in summer. Such information is useful for other

fields such as agriculture and hydropower energy to have more efficient water resources management. For example, Kumambala and Ervine (2010) reviewed the water resources related to Lake Malawi and Shire River and its sensitivity of future climate change using water balance models (e.g., Kebede et al., 2006). The diurnal variations in precipitation can influence the variables of water balance model such as rainfall, lake level and outflow from the lake directly. Therefore, our new findings in this study are informative to the community of water balance models for more accurate estimation of water resources of Lake Malawi.

This study is mainly a case study in only one particular year. Therefore, longer studies on the interaction of large-scale monsoon circulations with the diurnal cycle would be highly desirable. Further analysis should be undertaken on the climate variability of the large-scale monsoon circulation and its impacts on the diurnal cycle of precipitation, and the associated terrestrial hydrological processes. Thiery et al. (2016) have shown that the extreme rainfall due to Lake Victoria is modified by future climate change. Since Lake Victoria and Lake Malawi are located in the same tropical region, similar influence of lake-induced precipitation can be expected. Such insights can help mitigate natural disasters of flooding and drought in this region.

Acknowledgement

The authors greatly appreciate two reviewers, Dr. Ryan Teuling and Dr. Femke Jansen at Wageningen University for their quite constructive and useful comments on the manuscript. The computational resource of this study is supported by Norwegian High-Performance Computing Program resources (NN9039K, NS9039K, NN9385K, NS9207k). S. Koseki is supported by the European Union Seventh Framework Programme (EU-FP7/2007-2013) PREFACE (Grant Agreement No. 603521), ERC

619 STERCP project (Grant Agreement No. 648982), and from the Research Council of
620 Norway (233680/E10). P. A. Mooney gratefully acknowledges funding from the
621 Research Council of Norway (Grant No. 268243).
622

623 **Reference**

624 Bhatt, B. C., Sobolowski, S., and Higuchi, A.: Simulation of Diurnal Rainfall
625 Variability over the Maritime Continent with a High-Resolution Regional
626 Climate Model. *J. Meteorol. Soc. Jpn*., **94A**, 89-103,
627 doi:10.2151/jmsj.2015-052, 2016.
628 Bohlinger, P., Sorteberg, A., and Sodemann, H.: Synoptic conditions and
629 moisture sources actuating extreme precipitation in Nepal. *J. Geophys. Res.*
630 *Atmos*., **122**, 12,653-12,671, doi:10.1102/2017JD027543, 2017.
631 Bonan, G. B.: Forests and Climate Change: forcings, feedbacks and climate benefits
632 of forests. *Science*, **320**, 1444-1449, 2008.
633 Camberlin, P.: Rainfall Anomalies in the Source Region of the Nile and Their
634 Connection with the Indian Summer Monsoon. *J. Climate*, **10**, 1380-1392,
635 1997.
636 Chen, F., and Dudhia, J.: Coupling an advanced land-surface/hydrology
637 model with the Pen State/NCAR MM5 modeling system. PartI: model
638 description and implementation. *Mon. Wea. Rev*., **129**, 569-585, 2001a.
639 Chen, F., and Dudhia, J.: Coupling an advanced land-surface/hydrology
640 model with the Pen State/NCAR MM5 modeling system. PartII: model
641 validation. *Mon. Wea. Rev*., **129**, 587-604, 2001b.
642 Chen, F., and co-authors.: Description and Evaluation of the Characteristic of

the NCAR High-Resolution Land Data Assimilation. *J. Appl. Meteorol. Clim.*, **46**, 694-713, https://doi.org/10.1175/JAM2463.1, 2007.

Cook, B. I., Bonan, G. B., and Levis, S.: Soil Moisture Feedbacks to Precipitation in Southern Africa. *J. Climate*, **19**, 4198-4206, 2006.

Cosgrove, B. A., and co-authors.: Land surface model spin-up behavior in the North American Land Data Assimilation System (NLDAS). *J. Geophys. Res.*, **108**(D22), doi:10.1029/2002JD003316, 2002.

Crosman, E. T., and Horel, J. D.: Sea and Lake Breezes: A Review of Numerical Studies. *Boundary-Layer Meteorol.*, **137**, 1-29, doi:10.1007/s10546-010-9517-9, 2010.

Dee, D. P., and co-authors.: The ERA-Interim reanalysis: configuration and performance of the data assimilation system. *Q. J. Roy. Meteorol. Soc.*, **137**, 553-597, doi:10.1002/qj.828, 2011.

Diallo, I., Giorgi, F., and Stordal, F.: Influence of Lake Malawi on regional climate from a double-nested regional climate model experiment. *Clim. Dyn.*, **50**, 3397-3411, doi:10.1007/s00382-017-3811-x, 2018.

Diro, G. T., Raischer, S. A., Giorgi, F., and Tompkins, A. M.: Sensitivity to seasonal climate and diurnal precipitation over Central America to land and sea surface schemes in RegCM4. *Climate. Res.*, **52,** 31-48, doi:10.3354/cr01049, 2012.

Estoque, M. A.: The sea breeze as a function of the prevailing synoptic situation. *J. Atmos. Sci.*, **19**, 244-250, 1962.

Gleixner, S., Keenlyside, N. S., Demissie, T. D., Counillon, F., Wang, Y. and Viste, E.: Seasonal predictability of Kiremt rainfall in coupled general circulation models. *Environ. Res. Lett.*, **12**, 114016, 2017.

668 Hong, S. Y., and Lim, J. O. J.: The WRF single-moment 6-Class microphysics
669 scheme (WSM6). *J. Kor. Meteorol. Soc*., **42**, 129-151, 2006.
670 Hong, S. Y., and Dudhia, Y.: A new vertical diffusion package with an explicit
671 treatment of entrainment processes. *Mon. Wea. Rev*., **134**, 2318-2341, 2006.
672 Huffman, G. J., Bolvin, D. T., Nelkin, E. J., Wolff, D. B., Adler, R. F., Gu, G., Hong,
673 Y., Bowman, K. P., and Stocker, E. F.: The TRMM multisatellite
674 precipitation analysis (TMPA): Quasi-global, multiyear, combined-sensor
675 precipitation estimates at fine scales. *J. Hydrometeor*., **8**(1), 38-55, 2007.
676 Janjíc, Z.: The Step-Mountain Eta Coordinate Model: Further development of
677 the convection, viscous sublayer, and turbulence closure scheme.
678 *Mon. Wea. Rev*., **122**, 927-945, 1994.
679 Joseph, B., Bhatt, B. C., Koh, T.-Y., and Chen, S.: Sea breeze simulation over
680 Malay Peninsula over an intermonsoon period. *J. Geophys. Res*., **113**,
681 p.D20122, doi:10.1029/2008JD010319, 2008.
682 Jury, M. R.: Summer climate of Madagascar and monsoon pulsing of uts
683 vortex. *Meteorol. Atmos. Phys*., **128**, 117-129,
684 doi:10.1007/s00703-015-0401-5, 2016.
685 Kain, J. S.: The Kain-Fritsch convective parameterization: an update.
686 J. *Appl. Meteor*., **43**, 170-181, 2004.
687 Kebede, S., Travia, Y., Alemayechu, T., and Marc, V.: Water balance of Lake
688 Tana and its sensitivity to fluctuations in rainfall, Blue Nile basin, Ethiopia.
689 *J. Hydrol*., **316**, 233-247, 2006.
690 Keen, C. S., and Lyons, W. A.: Lake/Land Breeze Circulations on the Western
691 Shore of Lake Michigan. *J. Appl. Meteorol*., **17**, 1843-1855, 1978.
692 Kikuchi, K., and Wang, B.: Diurnal Precipitation Regimes in the Global

693 Tropics. *J. Climate*, **21**, 2680-2696, 2008.
694 Kitoh, A., and Arakawa, O.: Reduction in tropical rainfall diurnal variation by
695 global warming simulated by a 20-km mesh climate model.
696 *Geophys. Res. Lett*., **32**, L187709, doi:10,1029/2005GL023350, 2005.
697 Koseki, S., Koh, T.-Y., and Teo, C.-K.: Effects of the cold tongue in the South
698 China Sea on the monsoon, diurnal cycle, and rainfall in the Maritime
699 Continent. *Quart. J. Roy. Meteorol. Soc*., **139**,
700 1566-1582, doi:10.1002/qj2025, 2013.
701 Koseki, S., and Bhatt, B. C.: Unique relationship between tropical rainfall and
702 SST to the north of the Mozambique Channel in boreal winter.
703 *Int. J. Climatology*, **38** (S1), e378-e387, doi:10.1002/joc5378, 2018.
704 Koseki, S., Pohl, B., Bhatt, B. C., Keenlyside, N., and Nkwinkwa Njouodo, A. S.:
705 Insights into the summer diurnal cycle over eastern South Africa.
706 *Mon. Wea. Rev*., doi:10.1175/MWR-018-184-1, 2018.
707 Kruit, R. J. W., Holtslag, A. A. M., and Tijim, A. B. C.: Scaling of the sea-
708 breeze strength with observations in the Netherlands.
709 *Boundary-Layer Meteorol*., **112**, 369-380, 2004.
710 Kumambala, P. G., and Ervine, A.: Water Balance Model for Lake Malawi
711 and its Sensitivity to Climate Change.
712 *The Open Hydrology Journal*, **4**, 152-162, 2010.
713 Lauwaet, D., van Lipzig, N. P. M., Van Weverberg, K., De Ridder, K., and Goyens,
714 C.: The precipitation response to the desciccation of Lake Chad. *Quart. J. Roy.*
715 *Meteorol. Soc*., **138**, 707-719, 2012
716 Mak, M. K., and Walsh, J. E.: On the relative intensities of sea and land breezes.
717 *J. Atmos. Sci*., **33**, 242-251, 1976.

718 Mlawer, E., Taubman, S., Brown, P., Iacono, M., and Clough, S.: Radiative
719 transfer for inhomogeneous atmosphere: RRTM, a validated correlated-k
720 model for the long-wave. *J. Geophys. Res*., **102**, 16663-16682, 1997.
721 Mooney, P. A., Mulligan, F. J., and Broderick, C.: Diurnal cycle of
722 precipitation over the British Isles in a 0.44° WRF multiphysics regional
723 climate ensemble over the period 1990-1995. *Clim. Dyn*., **47**(9), 3281-3300,
724 doi:10.1007/s00382-016-3026-6, 2016.
725 Mooney, P. A., Broderick, C., Bruyere, C. L., Mulligan, F. J., and Prein, A. F.:
726 Clustering of Observed Diurnal Cycle of Precipitation over the United
727 States for Evaluation of a WRF Multiphysics Regional Climate Ensemble.
728 *J. Climate*, **30** (22), doi:10.1175/JCLI-D-16-0851.1, 2017.
729 Neuland, H.: Abnormal high water levels of Lake Malawi?- An attempt to
730 assess the future behaviour of the lake water levels. *Geo J*., **9**, 323-334, 1984.
731 Nikulin and co-authors.: Precipitation Climatology in an Ensemble of
732 CORDEX-Africa Regional Climate Simulations. *J. Climate*, **25**, 6057-6078,
733 2012.
734 Notaro, M., Holman, K., Zarrin, A., Fluck, E., Vavrus, S., and Bennington, V.:
735 Infleuence of the Laurentian Great Lakes on Regional Climate. *J. Climate*, **26**,
736 789-804, 2013.
737 Pielke, R. A.: Influence of the spatial distribution of vegetation and soils on the
738 prediction of cumulus convective rainfall. *Rev. Geophys*., **39**, 151-177,
739 doi:https//doi.org/10.1029/1999RG000072, 2001.
740 Pitman, A. J., Avila, F. B., Abramowitz, G., Wang, Y. P., Phipps, S. J., and de
741 Noblet-Ducoudré, N.: Importance of background climate in determing impacts
742 of land-cover change on regional climate. *Nature Climate Change*, **1**, 472-475,

743 doi:10.1038/NCLIMATE1294, 2011.
744 Pohl, B., Rouault, M. and Roy, S. S.: Simulation of the annual and diurnal
745 cycles of rainfall over South Africa by a regional climate model. *Clim. Dyn*.,
746 **43**, 2207-2226, doi:10.1007/s00382-013-2046-8, 2014.
747 Reynolds, R. W., Smith, T. M., Liu, C., Chelton, D. B., Casey, K. S., and Schlax, M.
748 G.: Daily high-resolution-blended analyses for sea surface temperature.
749 *J. Climate*, **20**, 5437-5496, doi:10.1175/2007JCL1824, 2007.
750 Semazzi, F. H. M., and Song, Y.: A GCM study of climate change induced by
751 deforestration in Africa. *Climate Research*, **17**, 169-182, 2001.
752 Schäfer, M. P., Ottfried, D., and Bniface, M.: Streamflow and lake water level
753 changes and their attributed causes in Eastern and Southern Africa: state of the
754 art review. *Int. J. Water Resour. D*., **6**,
755 853-880, doi:10.1080/07900627.2015.1091289, 2015.
756 Segele, Z. T., Lamb, P. J., and Leslie, L. M.: Large-scale atmospheric
757 circulation and global sea surface temperature associations with Horn of
758 Africa June-September rainfall. *Int. J. Climatology*, **29**(8), 1075-1100, 2009a.
759 Skamarock, W. C., Klemp, J. B., Dudhia, J., Gill, D. O., Barker, D. M., Duda, M.,
760 Huang, X. Y., Wang, W., and Powers, J. G.: A description of the
761 advanced research WRF version 3. *NCAR technical note*,
762 NCAR/TN/u201345?STR, 123pp, 2008.
763 Skofronick-Jackson, G., and co-authors.: The Global Precipitation
764 Measurement (GPM) Mission for Science and Society. *Bull. Amer. Meteoro.*
765 *Soc*., 1679-1696, doi:10.1175/BAMS-D-15-00306.1, 2017.
766 Sousounis, P. J., and Mann, G. E.: Lake-Aggregate Mesoscale Disturbances. PartV:
767 Impacts on Lake-Effect Precipitation. *Mon. Wea. Rev*., **128**, 728-745, 2000.

768 Steyn, D. G.: Scaling the vertical structure of sea breezes revisited.
769 *Boundary-Layer Meteorol.*, **107**, 177-188, 2003.
770 Stivari, S. M. S., de Oliveira, A. P., Karam, H. A., and Suares, J.: Patterns of
771 Local Circulation in the Itaipu Lake Area: Numerical Simulations of Lake
772 Breeze. *J. Appl. Meteorol.*, **42**, 37-50,
773 doi:10.1175/1520-0450(2003)<0037:POLCIT>2.0.CO;2, 2003.
774 Sugimoto, S., and Takahashi, H. G.: Seasonal Differences in Precipitation Sensitivity
775 to Soil Moisture in Bangladesh and Surround Regions. *J. Climate*, **30**, 921-
776 938, doi:10.1175/JCLI-D-15-0800.1, 2017.
777 Teo, C.-K., Koh, T.-Y., Lo, J. C. F., and Bhatt, B. C.: Principal component
778 analysis of observed and modeled diurnal rainfall in the Maritime Continent.
779 *J. Climate*, **24**, 4662-4675, 2011.
780 Thiery, W., Davin, E. L., Seneviratne, S. I., Bedka, K., Lhermitte, S., and van Lipzig,
781 N. P. M.: Hazardous thunderstorm intensification over Lake Victoria. *Nat.*
782 *Communication*, **7**, 12786.
783 Tyson, D. P.: Nocturnal local winds in a Drakensberg Valley.
784 *South African Geographical Journal*, **50**, 15-32, 1968a.
785 Tyson, D. P.: A Note on the Nomenclature of the Topographically-induced
786 Local Winds of Natal. *South African Geographical Journal*, **50**, 33-34, 1968b.
787 Viste, E., and Sorteberg, A.: The effect of moisture transport variability on
788 Ethiopian summer precipitation. *Int. J. Climatology*, **33**, 3106-2123,
789 doi:10.1002/joc.3566, 2013.
790 Walker, J., and Rowntree, P. R.: The effect of soil moisture on circulation and rainfall
791 in a tropical model. *Quart. J. Roy. Meteorol. Soc.*, **103**, 29-46, 1977.
792 Wely, O. L. F., Ribbink, A. J. and Tweddle, D.: Lake Malawi: fishes, fisheries,

biodiversity, health and habitat. *Aquat. Ecosyst. Health Manag*., **13**:3, 241-254, doi:10.1080/14634988.2010.504695, 2010.

Xu, L., Liu, H., Du, Q., and Wang, L.: Evaluation of the WRF-lake model over a highland freshwater lake in southwest China. *J. Geophys. Res. Atmos*., **121**, 13,989-14,005, doi:10.1002/2016JD025396, 2016.

Yang, G., and Slingo, J.: The diurnal cycle in the tropics. *Mon. Wea. Rev*., **129**, 784-801, doi:10.1175/1520-0493(2001)129<0784:TDCITT>2.0CO;2, 2001.

Figures

(a)

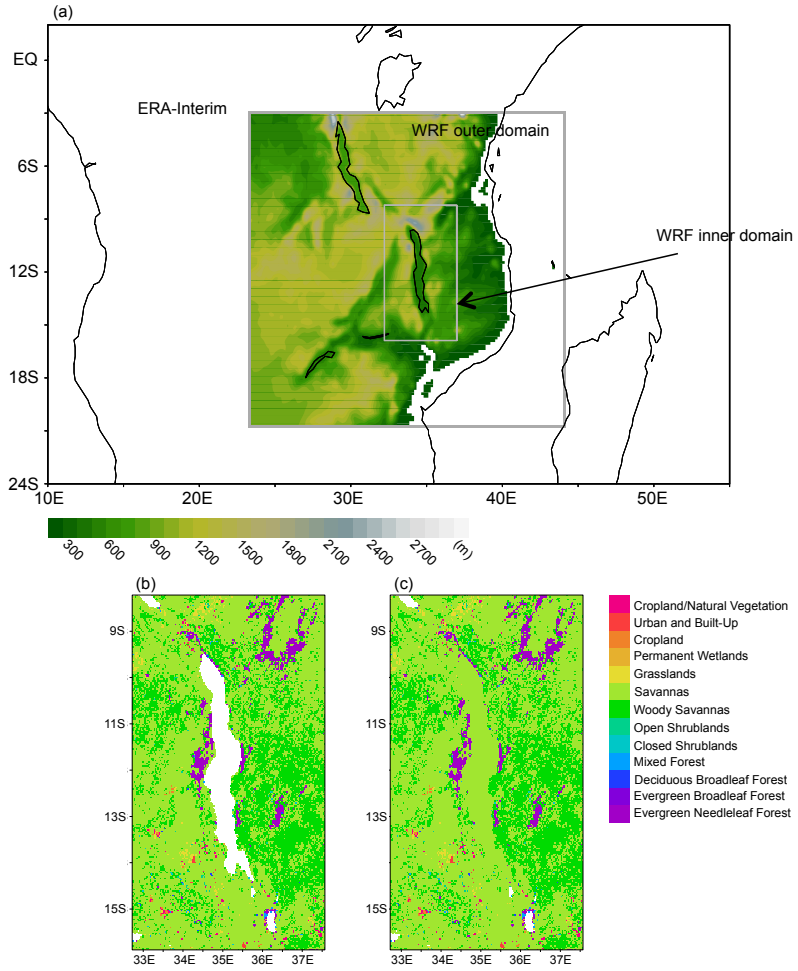

Figure 1.
(a) Domains for WRF simulations with terrain height obtained from GTOPO30. (b) and (c) landuse index of the boundary condition for the inner domain of WRF-CTL and WRF-NOLM, respectively

804

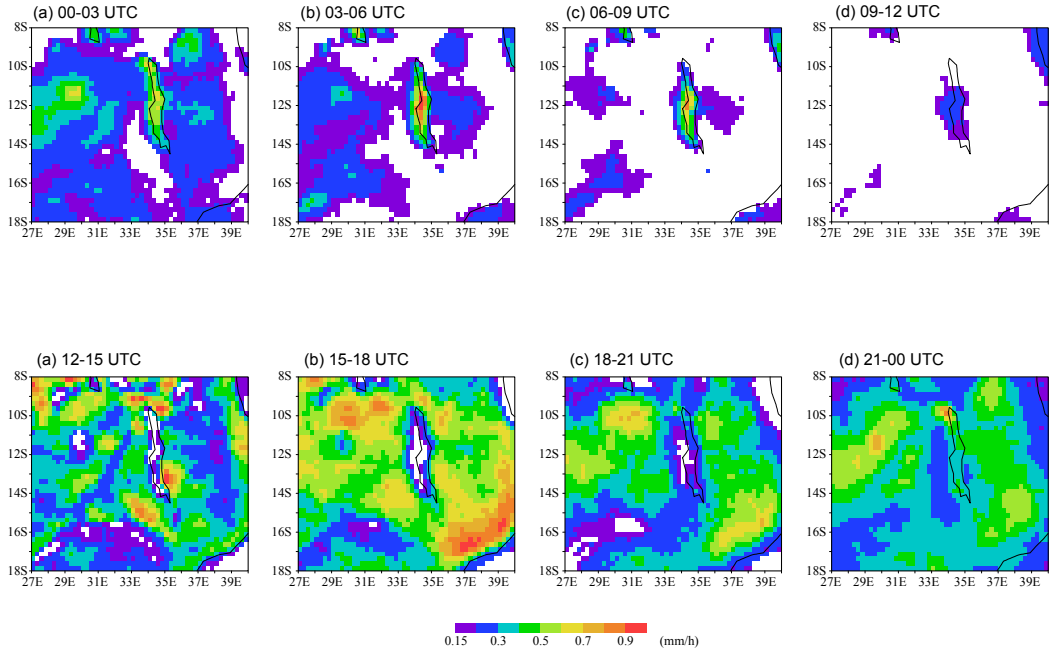

Figure 2.
Climatological 3-hourly precipitation of TRMM-3B42 in NDJFM (1998-2012). The white color is precipitation less than 0.15mm/h.

805

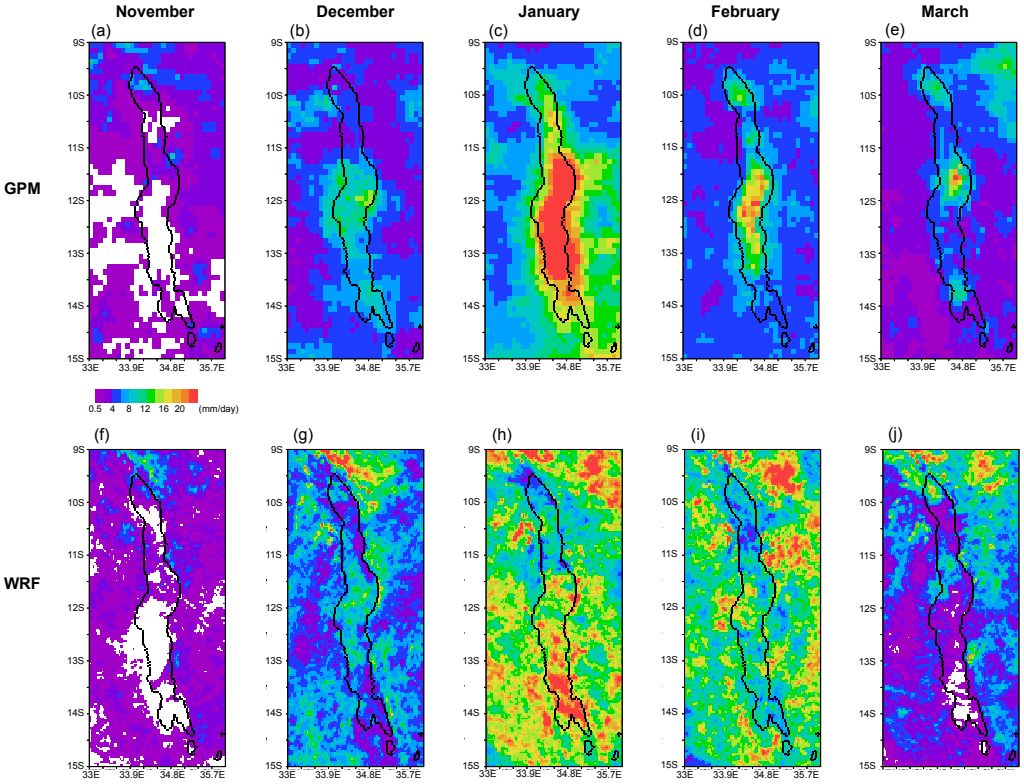

Figure 3.
Monthly-mean precipitation of (top) GPM and (bottom) WRF-CTL from November to March in 2014/15. The white color is precipitation less than 0.5 mm/day.

806

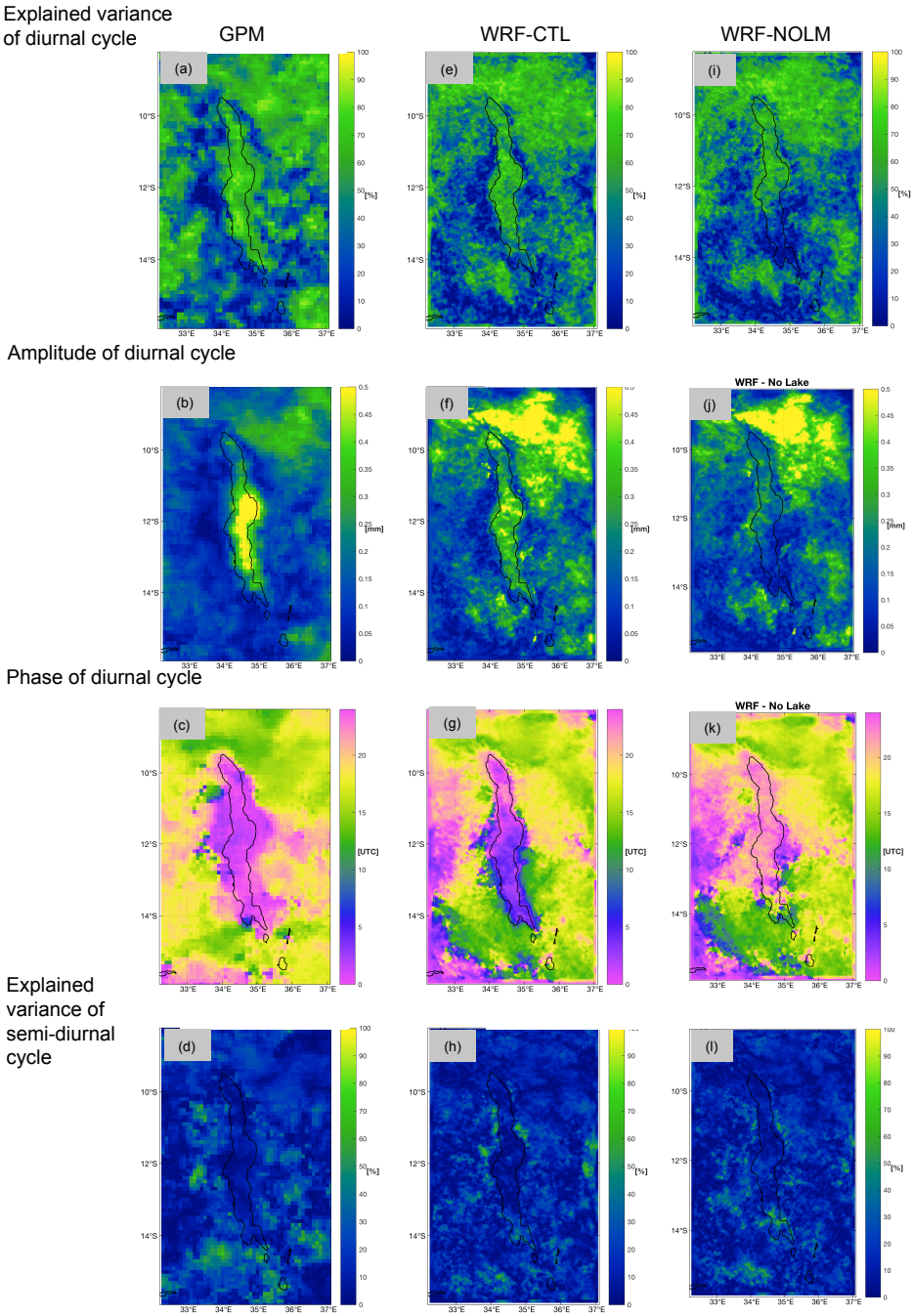

Figure 4.
Characteristics of daily-scale temporal variation in precipitation estimated by harmonic analysis for (1st row) explained variance of diurnal cycle, (2nd row) amplitude of diurnal cycle, (3rd row) phase of diurnal cycle, and (4th row) explained variance of semi-diurnal cycle for (left) GPM, (middle) WRF-CTL, and (right) WRF-NOLM, respectively.

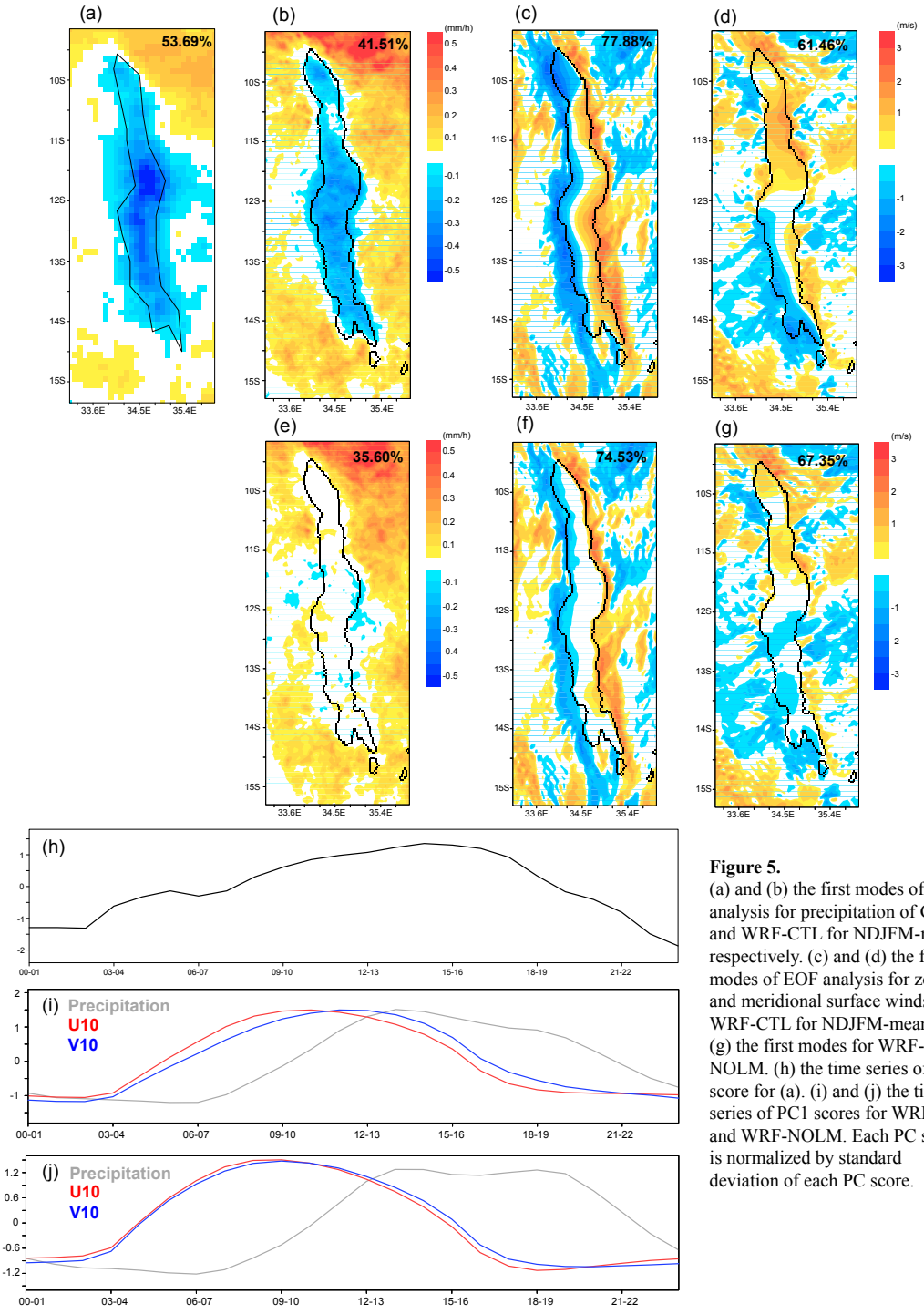

Figure 5.
(a) and (b) the first modes of EOF analysis for precipitation of GPM and WRF-CTL for NDJFM-mean, respectively. (c) and (d) the first modes of EOF analysis for zonal and meridional surface winds of WRF-CTL for NDJFM-mean. (e)-(g) the first modes for WRF-NOLM. (h) the time series of PC1 score for (a). (i) and (j) the times series of PC1 scores for WRF-CTL and WRF-NOLM. Each PC score is normalized by standard deviation of each PC score.

813

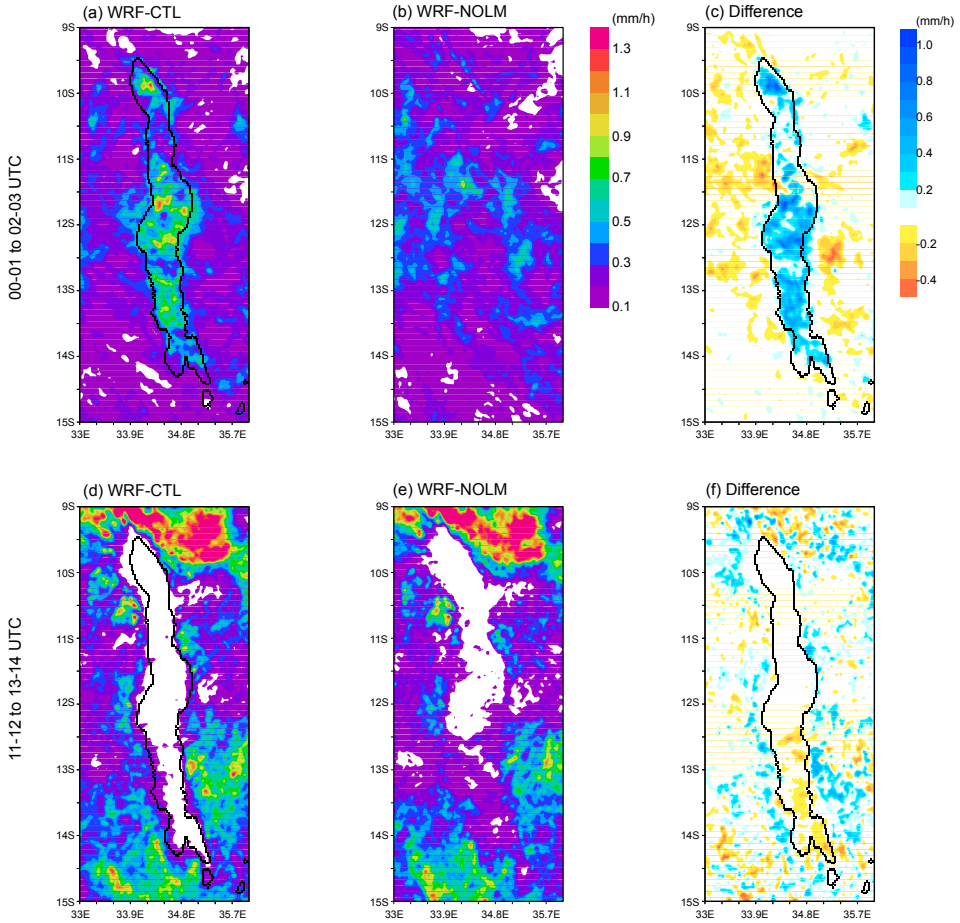

Figure 6.
Nighttime mean of precipitation of WRF-CTL and WRF-NOLM in (a) and (b), respectively and its difference (WRF-CTL minus WRF-NOLM) in (c). (d)-(f) same as (a)-(c), but for daytime mean.

814

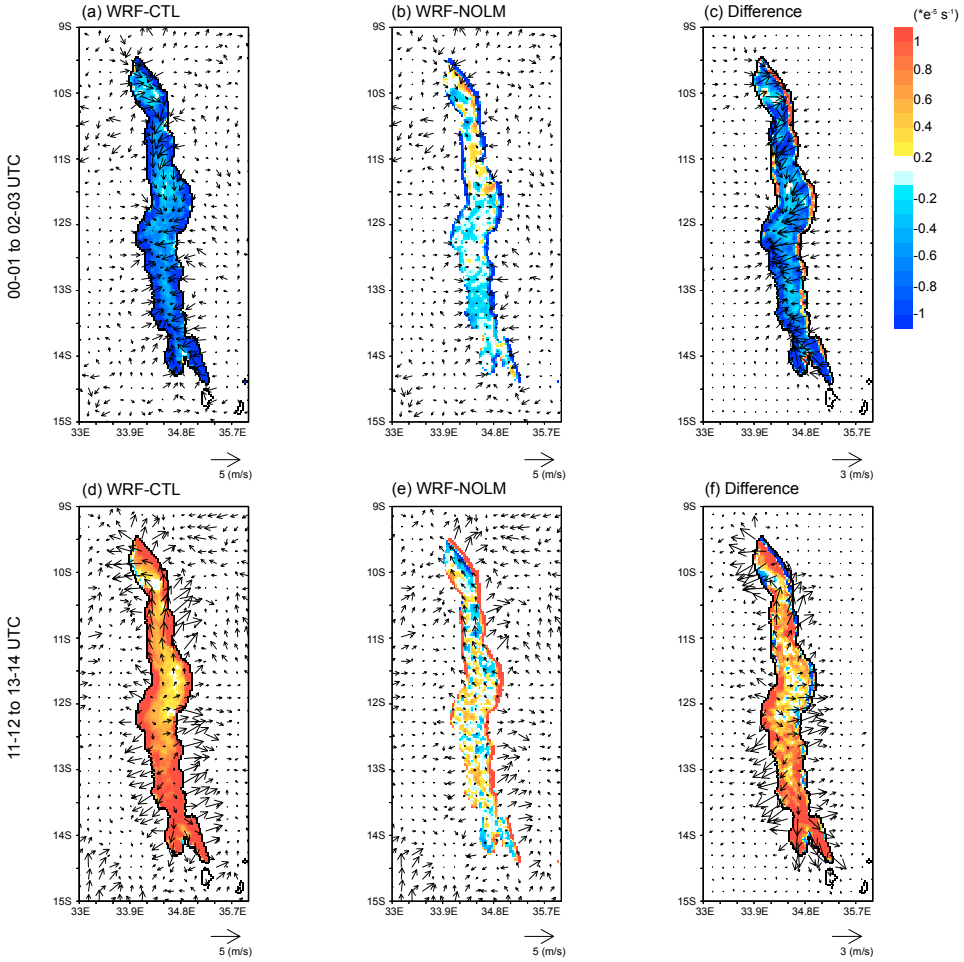

Figure 7.
Same as Fig.6, but for surface horizontal winds (arrows) and its divergence (color). Note that the surface winds and its divergence are anomalies from daily-mean values.

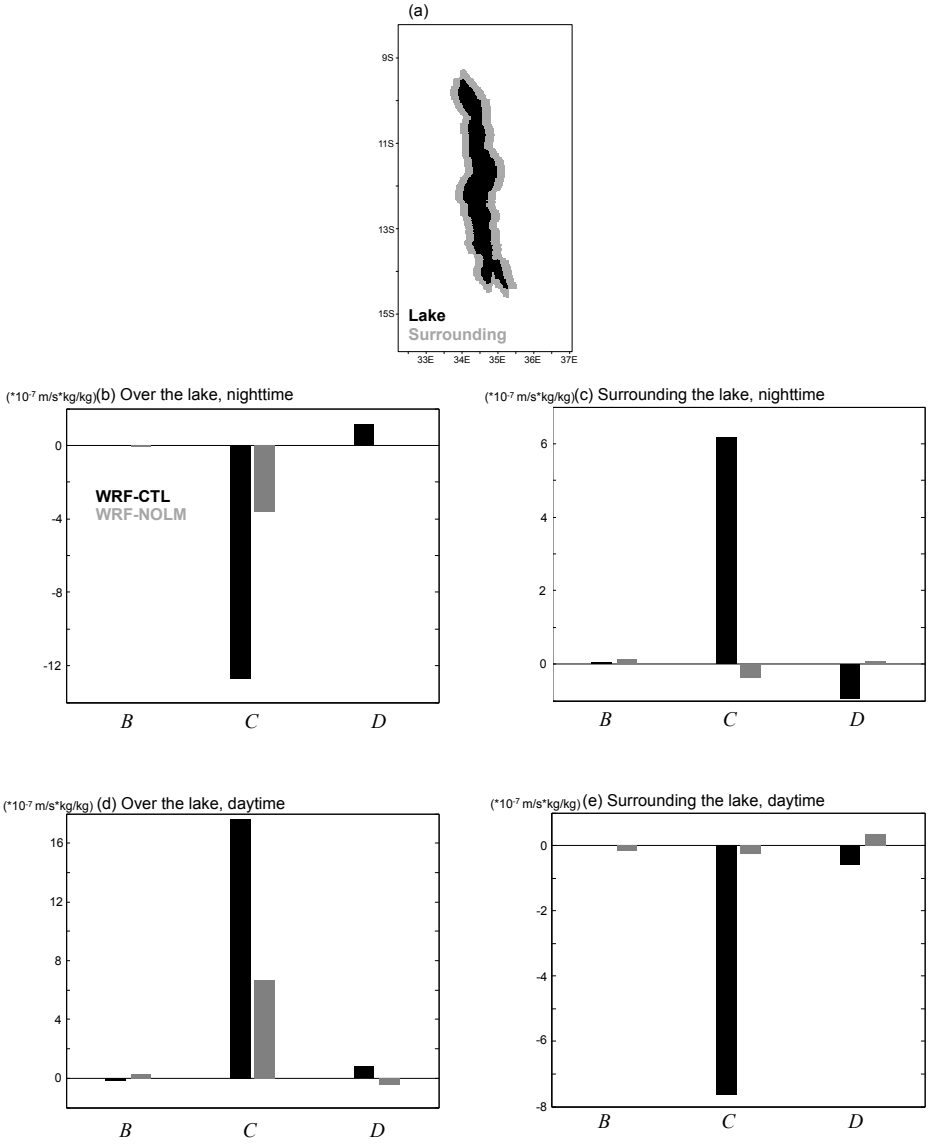

Figure 8.
(a) Grids of the lake (black) and surrounding area (gray) for area-averaging. The area-averaged three components of moisture flux divergence in the equation 3 for (b) over the lake, nighttime (00-01 to 02-03 UTC), (c) surrounding the lake, nighttime, (d) over the lake, daytime (11-12 to 13-14 UTC), and (e) surrounding the lake, daytime for WRF-CTL (black) and WRF-NOLM (gray), respectively.

819

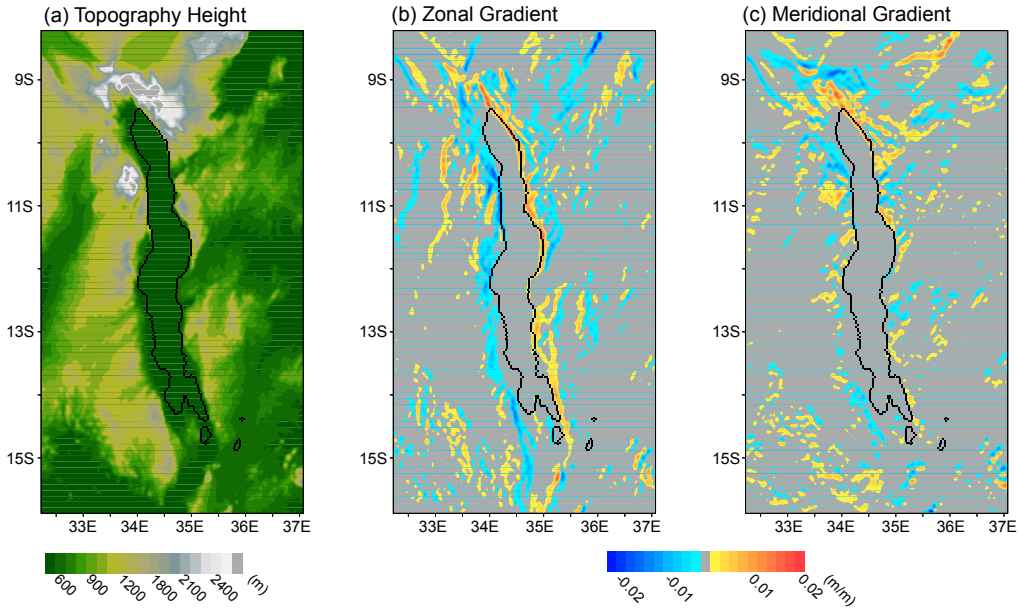

Figure 9.
The distribution of topography around Lake Malawi. (a) Topographic altitude in WRF inner domain and its zonal and meridional gradients in (b) and (c).

820